Hindawi Publishing Corporation
International Journal of Antennas and Propagation
Volume 2015, Article ID 940212, 8 pages
http://dx.doi.org/10.1155/2015/940212

Research Article

Sub-Millimeter-Wave 10 dB Directional Coupler Based on Micromachining Technique

Shuang Liu,[1] Jiang Hu,[1] Yong Zhang,[1] Yupeng Liu,[1] Tianhao Ren,[1] Ruimin Xu,[1] and Quan Xue[2]

[1] *School of Electronic Engineering, University of Electronic Science and Technology of China, Chengdu 611731, China*
[2] *Department of Electronic Engineering, City University of Hong Kong, Kowloon, Hong Kong*

Correspondence should be addressed to Shuang Liu; ranranshuangshuang@163.com

Received 26 August 2015; Accepted 21 October 2015

Academic Editor: Herve Aubert

Copyright © 2015 Shuang Liu et al. This is an open access article distributed under the Creative Commons Attribution License, which permits unrestricted use, distribution, and reproduction in any medium, provided the original work is properly cited.

A waveguide 10 dB directional coupler operating from 325 GHz to 400 GHz is designed based on the short-slot Riblet-type coupling configuration and fabricated using the deep reactive ion etching (DRIE) silicon micromachining technique. The skin depth and the conductivity of the gold film with the roughness of 0.2 μm are investigated at 300~1000 GHz frequency band for the higher accuracy. In order to measure the small-size four-port coupler using the two-port VNA with big-size flanges, three testing topologies are designed, in which the terahertz (THz) wedged-type absorbing material terminals are adopted as the waveguide matching loads. The measured average insertion loss is 0.5 dB after deducting the intrinsic loss and the measured average isolation is better than 25 dB, which are in good agreement with simulations. The analysis and the design are verified to be accurate and valuable for the high-performance sub-millimeter-wave waveguide components.

1. Introduction

Sub-millimeter-wave waveguide components have advantages over the planar transmission line components due to their lower losses, higher power handling capacities, and ease of interconnection with the measurement system and other solid-state systems. In this paper, a 10 dB directional coupler based on the H-plane waveguide short-slot Riblet-type coupling configuration with two apertures is presented at the 325~400 GHz frequency band.

Because the conductivity and the skin depth of the bulk metal are altered under the influence of the frequency and the surface roughness while the frequency increases, they are investigated for obtaining more accurate loss at the 100~1000 GHz frequency band.

Because the straight waveguide loss cannot be ignored when the frequency is up to 300 GHz [1], the length of the input/output straight waveguide should be kept as short as possible for less loss. However, it is difficult to measure all characteristics of the four-port coupler with small-size using the two-port VNA with big-size flanges. Therefore, three testing topologies based on the same Riblet-type coupling configuration are designed for measurements.

Because the micromachining techniques have the advantage over the computer numerical control (CNC) metal machining due to their highly accurate dimensional control [2], the silicon DRIE micromachining is adopted for the fabrication of the proposed coupler. The measured results are in good agreement with the simulations, which verifies that the accuracy of the analysis above and the design process is valuable to realize high-performance waveguide components at the sub-millimeter-wave frequency band.

2. Design and Simulation

2.1. The Design of the Coupler. While the frequency is higher than 300 GHz, the design of the waveguide component is hampered enormously by the influence of the fabrication tolerance. The good solution is selecting a much simpler

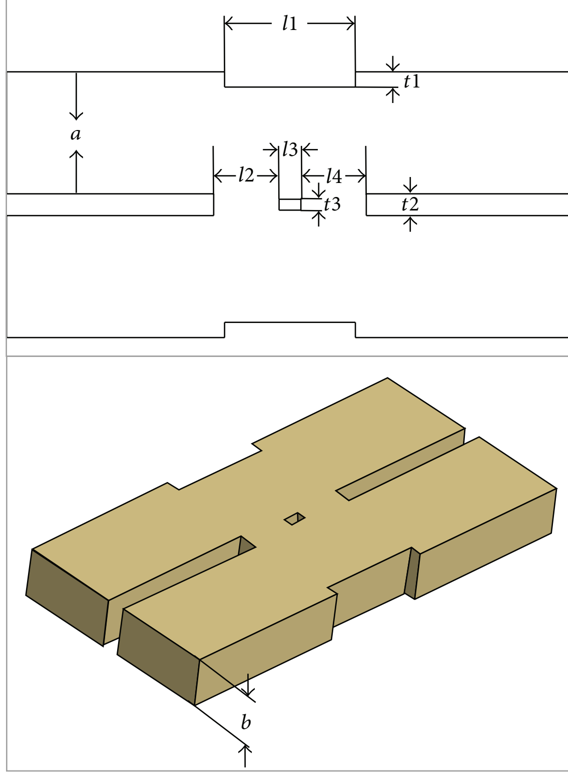

Figure 1: Schematic of the basic structure in the coupler.

Table 1: Optimized dimensions of the 10 dB directional coupler.

a	559 μm	$l2$	300 μm	$t1$	70 μm
b	279 μm	$l3$	100 μm	$t2$	100 μm
$l1$	600 μm	$l4$	300 μm	$t3$	50 μm

structure for obtaining the given performance. Compared with the E-plane branch-line configuration, the H-plane short-slot Riblet-type configuration [3] has simpler structure and wider bandwidth, which is adopted as the basic structure of the directional coupler.

The basic structure of the directional coupler is shown in Figure 1. Different coupling coeffecient can be obtained by adjusting the dimensions ($l3$, $t3$) of the coupler apertures under the premise of the same length of the coupling region. The quasi-ridge structure is adopted in the coupling area for getting better return loss. To simplify the fabrication, the etching depth of the whole couple is set to an equal value. In order to make it easier to connect with external circuits, the standard WR-2.2 rectangular waveguides with the size of 559 μm × 279 μm are used as the input and output waveguides. The optimized dimensions using the commercial full-wave electromagnetic simulation software (ANSYS HFSS) are shown in Table 1.

2.2. The Analysis of the Skin Depth and Metal Conductivity. According to the time-varying electromagnetic theory, the properties of bulk metal thin films with more than several

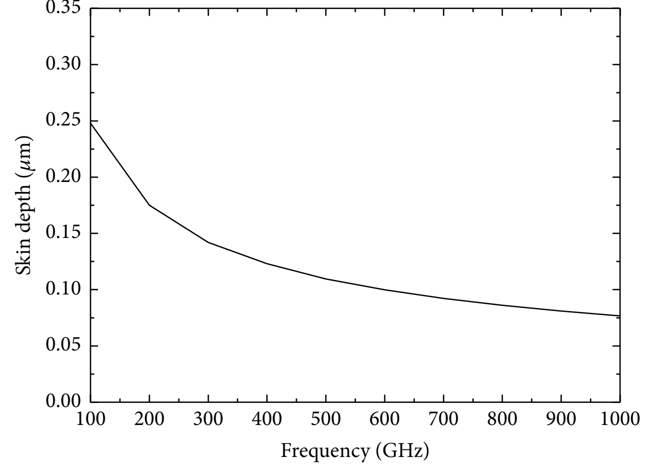

Figure 2: The skin depth of the smooth gold film at 100~1000 GHz.

tens of nm thickness are well described by the Drude model [4, 5], in which the conductivity σ is dependent on the angular frequency ω as follows:

$$\sigma(\omega) = \frac{\sigma_0}{1 + j\omega\tau}, \quad (1)$$

where $\sigma_0 = n_0 e^2 \tau / m^*$ is the intrinsic bulk conductivity at direct current and is also adopted in the ANSYS HFSS, $\omega = 2\pi f$ is the angular frequency, n_0, e, and m^*, respectively, denote the free electron density, the electronic charge, and the effective mass of the electrons, and τ refers to the scattering relaxation time of the free electron (i.e., $\tau = 27.135$ fs in [6], $\tau = 18.5$ fs in [7]).

According to the classical relaxation-effect model, the surface impedance $Z(\omega)$ and the skin depth δ of homogeneous metals with smooth surfaces are related to the complex conductivity $\sigma(\omega)$ by [8]

$$Z(\omega) = \sqrt{\frac{j\omega\mu_0\mu_r}{\sigma(\omega) + j\omega\varepsilon}}, \quad (2)$$

$$\delta = \frac{1}{\operatorname{Re}\{j\omega\mu_0\mu_r / Z(\omega)\}}, \quad (3)$$

where μ_0 is the permeability of free space; μ_r is the relative permeability; and ε is the permittivity. According to formula (3), the skin depth of the smooth gold film is shown in Figure 2.

From Figure 2, the skin depth of gold thin films with smooth surfaces is about 125~140 nm in the frequency band of 325~440 GHz.

When the surface roughness exceeds the skin depth of metals with smooth surfaces, the Hammerstad and Bekkadal model [9, 10] is adopted for predicting the loss due to

the rough metal surfaces. The attenuation constant of the rough metal surface $\alpha(\Delta_r)$ can be captured by a frequency dependent correction factor f_{rough} as in [11]

$$\alpha(\Delta_r) = \alpha(\Delta_r = 0) \times f_{\text{rough}}, \quad (4)$$

where $f_{\text{rough}} = 1 + (2/\pi)\arctan[1.4(\Delta_r/\delta)^2]$ and Δ_r = surface roughness.

Applying the concept of second-order small-perturbation method (SPM) based on first-principle classical electrodynamics [12–16], the frequency dependent conductivity due to surface roughness can be captured as follows:

$$\sigma(\Delta_r) = \frac{\sigma(\Delta_r = 0)}{f_{\text{rough}}^2}. \quad (5)$$

Taking account of practical situation, the waveguide surface is metallized by electroplating gold film layer with thickness of 3 μm which will be illustrated in Section 3, whose surface roughness is given by 0.2 μm. According to formula (5), the effective conductivity of the gold film with the roughness of 0.2 μm is shown in Figure 3.

From Figure 3, the effective conductivity is about 1.24×10^7 S/m at the frequency band of 325~400 GHz.

2.3. The Design Consideration for Measurements. According to the observation in [1], the insertion loss of a straight waveguide fabricated by the DRIE technology is about 0.4 dB/mm in the band of 325~440 GHz, which cannot be ignored when the operating frequency is increased to 300 GHz or higher. Hence, the whole size of the directional coupler should be kept as small as possible. However, measuring a four-port waveguide coupler using a two-port VNA with standard flanges of big size is difficult. To deal with this issue, three testing topologies with much shorter extended port waveguides, which can lead to less loss, are designed for measuring the *S*-parameter characteristics of the coupler, respectively, as shown in Figure 4. Because the distance (about 5.5 mm) between two under test ports is shorter than the lengths of two screws used in measurement flanges, which will cause collision of two screws, two under test ports are set in a line for convenient connection. To ensure the good matching of untested ports, two untested ports are turned to the orthogonal direction.

For the untested ports, conventional waveguide matching loads with big size cannot be used because it will lead to a longer extended waveguide and more loss. Therefore, THz wedged-type absorbing materials shown in Figure 5 are adopted as the replacement of matching loads. A single-port test fixture with standard WR-2.2 rectangular waveguide is fabricated for measurements, in which the absorbing material is set at the end of the H-plane waveguide as shown in Figure 5. The measured result is shown in Figure 6, in which the average return loss is better than 20 dB from 325 GHz to 400 GHz.

The simulated results of the three testing topologies with the analysis above are shown in Figures 12, 13, and 15.

3. Fabrication

As shown in Figure 7, the main micromachining process consists of the following steps. The whole testing structure is etched to a depth of 282 μm using the DRIE process on a polished silicon wafer with a thickness of 500 μm and another polished silicon wafer with the same thickness is used just as a cover. This procedure can avoid position error of interwafer bonding completely, which is crucial to the filter's performance. Then, the surfaces of the two etched wafers are both metallized by electroplating gold layer to a thickness of 3 μm. However, there is a problem that if there is a little gap between the upper and lower cavities it will lead to dramatic deterioration on the performance of filter. The problem is solved by the gold-to-gold compression bonding process due to its close bonding. Finally, to ensure the good electric connection to the measurement system, the end surfaces of the bonded testing structure are sputtered with a gold film of several nanometers.

The photographs of the three micromachined testing topologies are shown in Figure 8, where sizes of the three test topology are all given by 5.5 mm × 5.5 mm × 1 mm.

The standard UG-387 flange is most widely used in the millimeter-wave frequency band. However, dimensional tolerances of this waveguide flange impose a major limitation on precise measurements above 100 GHz. Instead, the modified ring-centered flanges with smaller alignment dowels are adopted in the text fixtures, as shown in Figure 9, which show a repeatability superior to that of the standard UG-387 flange [17]. As shown in Figure 10, test fixtures are fabricated to fit in the wafer testing structures so that they can be connected to the measurement system. THz wedged-type absorbing materials are stuffed into untested waveguide ports for the matching.

4. Measurements and Results

S-parameter measurements are carried out using Agilent N5245A VNA with OML 325~500 GHz frequency extenders, as shown in Figure 11. At first, the system is calibrated at the frequency range of 325~400 GHz by TRL standards with the insert loss less than 0.1 dB and the return loss better than 30 dB. And then the fixture with the silicon block is connected with standard WR-2.2 rectangular waveguides of frequency extenders.

The measures results of the through coupling topology and the parallel coupling topology are presented in Figures 12 and 13, which are compared to simulations. The measured coupling coefficient is about 10 dB with the loss less than 1 dB and the average return loss is better than 17 dB, which fits perfectly the simulations. Therefore, it verifies that the analysis and the designs in Section 2 are accurate. As shown in Figure 14, a straight waveguide with a length of 5.5 mm fabricated using the same DRIE process has been measured as well, whose average loss is about 0.25 dB/mm.

The measured isolation shown in Figure 15 has similar curve to the simulation. However, the value of the isolation deteriorates a little. The angle of the waveguide sidewall was measured to be 91.2° relative to the wafer surface due to

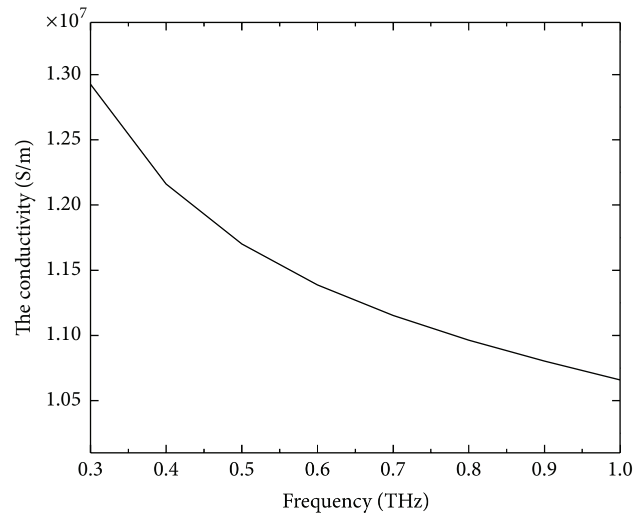

Figure 3: The conductivity of the gold thin film with surface roughness of 0.2 μm at the 300~1000 GHz frequency band.

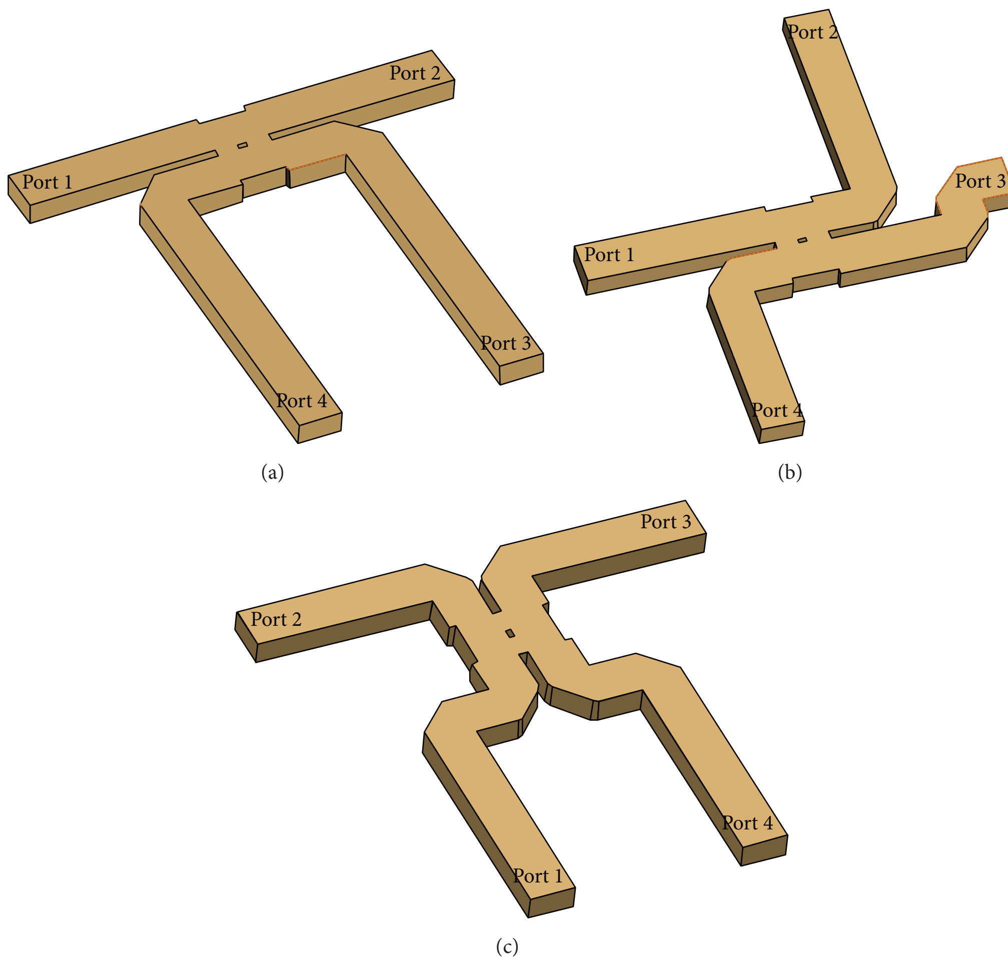

Figure 4: Testing topologies of the proposed coupler. (a) The through coupling topology (for testing the through coupling characteristic, in which the under test ports (port 1 and port 2) are set in a line and the untested ports (port 3 and port 4) are turned to the orthogonal direction). (b) The parallel coupling topology (for testing the coupling coefficient, in which the under test ports (port 1 and port 3) are set in a line and the untested ports (port 2 and port 4) are turned to the orthogonal direction). (c) The isolation topology (for testing the isolation characteristic, in which the under test ports (port 2 and port 3) are set in a line and the untested ports (port 1 and port 4) are turned to the orthogonal direction).

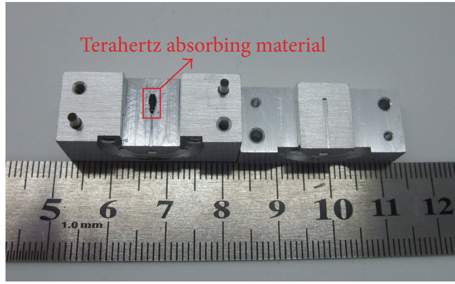

Figure 5: The text fixture with the THz absorbing material.

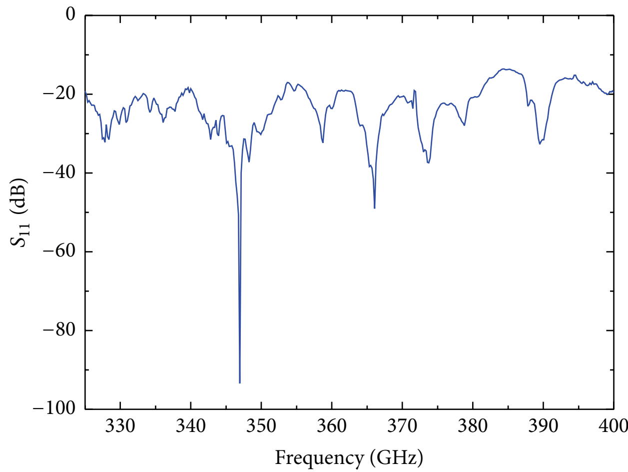

Figure 6: The measured return loss of the THz absorbing material.

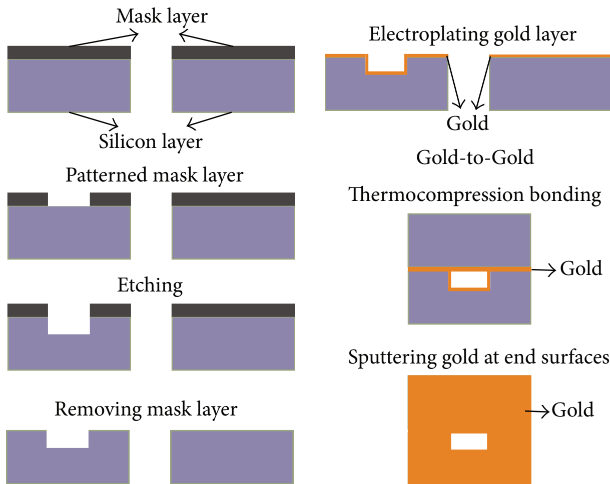

Figure 7: Main micromachining process.

the transverse etching in the DRIE process, which is the first reason of the deterioration. The second reason is the dimension deviation, as shown in Table 2. According to the analysis in Section 2, the untested ports are not matched perfectly using absorbing materials, which is the third reason. The fourth reason of the deterioration is coming from the

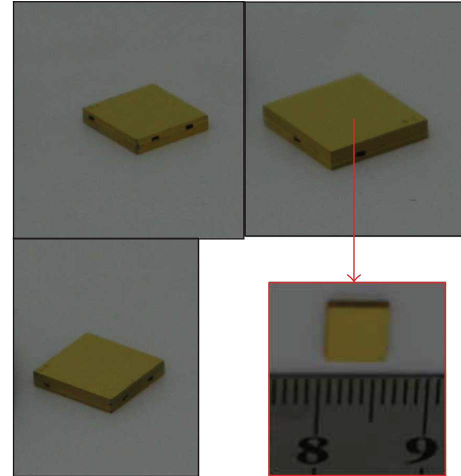

Figure 8: Photographs of testing topologies fabricated using DRIE on silicon wafers, with inner and outer surface metallization.

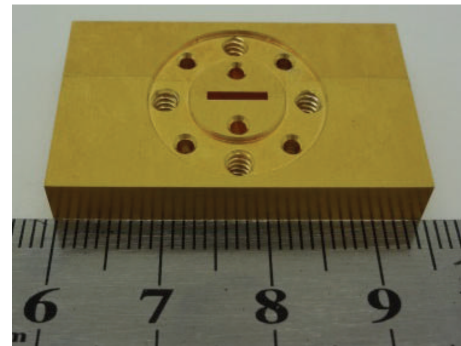

Figure 9: Test fixtures with the modified ring-centered flanges.

Table 2: Measured dimensions of the 10 dB directional coupler.

a	560 μm	$l2$	301 μm	$t1$	71 μm
b	282 μm	$l3$	99 μm	$t2$	99 μm
$l1$	598 μm	$l4$	301 μm	$t3$	51 μm

nonclose connection between the two end surfaces of the measurement setup and of the micromachined filter.

5. Conclusions

In this paper, a waveguide 10 dB directional coupler is fabricated by the DRIE micromachining technology. Because the effective conductivity and the skin depth of the gold film are altered under the influence of the frequency and the surface roughness, they are analyzed for obtaining more accurate insertion loss. Three test topologies are used for measurements. The measured results are in good agreement with the simulations, which certifies the accuracy of the design. The analysis in this paper offers the potential for more accurate designs of silicon micromachined components at sub-millimeter-wave frequency in the future.

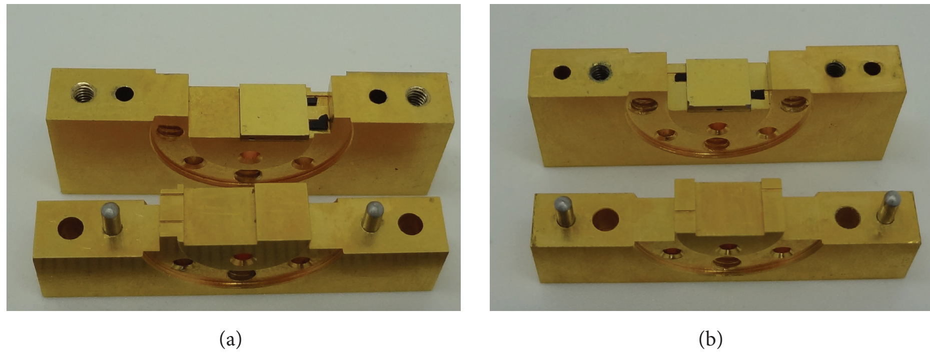

Figure 10: Test fixtures (a) for measuring the isolation topology and the through coupling topology (b) for measuring the parallel coupling topology.

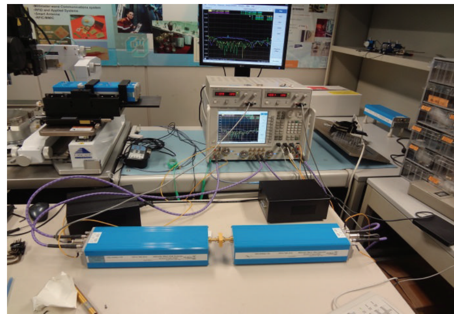

Figure 11: 325~500 GHz S-parameter measurement setup.

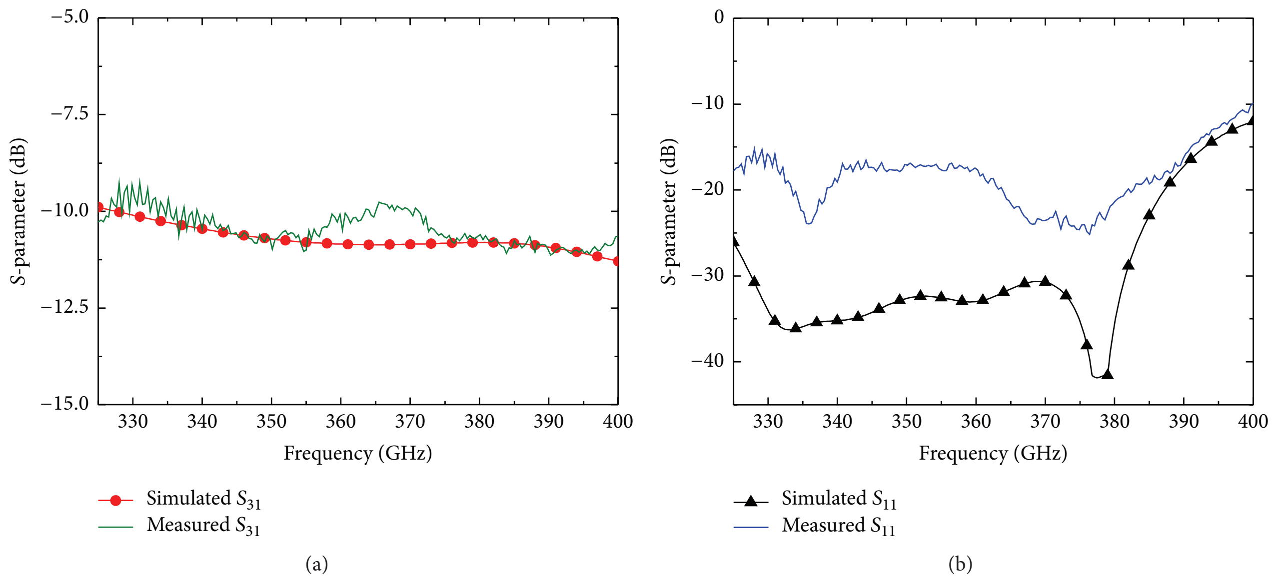

Figure 12: Measured (a) S_{31} and (b) S_{11} compared with measured and simulated results of the parallel coupling topology.

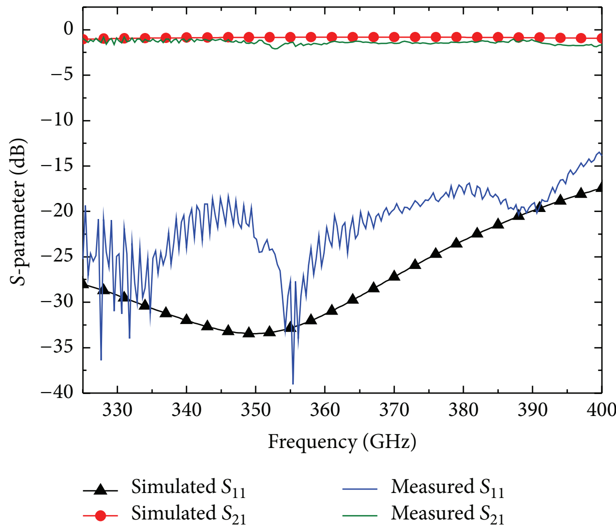

FIGURE 13: Measured S-parameter compared with measured and simulated results of the through coupling topology.

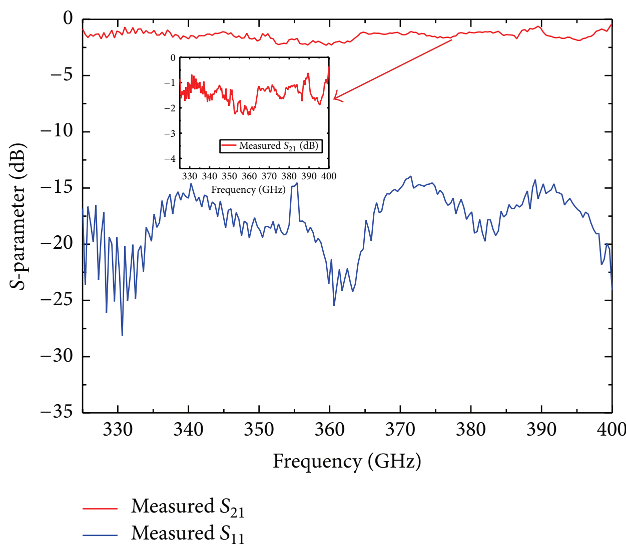

FIGURE 14: Measured results of the straight waveguide with length of 5.5 mm fabricated using the same DRIE process.

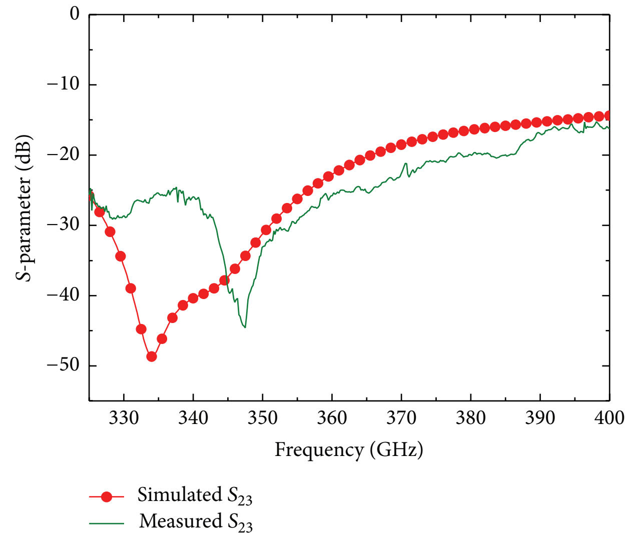

FIGURE 15: Measured S-parameter compared with measured and simulated results of the isolation topology.

Conflict of Interests

The authors declare that there is no conflict of interests regarding the publication of this paper.

Acknowledgments

The authors would like to thank Haotian Zhu and Peng Wu, Department of Electronic Engineering, City University of Hong Kong, for the measurement and helpful discussion. This work was supported by the National Natural Science Foundation of China (G0501020161371054).

References

[1] J. Hu, S. Xie, and Y. Zhang, "Micromachined terahertz rectangular waveguide bandpass filter on silicon-substrate," *IEEE Microwave and Wireless Components Letters*, vol. 22, no. 12, pp. 636–638, 2012.

[2] C. Jung-Kubiak, J. Gill, T. Reck et al., "Silicon microfabrication technologies for THz applications," in *Proceedings of the 17th IEEE Silicon Nanoelectronics Workshop (SNW '12)*, pp. 1–2, IEEE, Honolulu, Hawaii, USA, June 2012.

[3] H. Riblet, "The short-slot hybrid junction," *Proceedings of the Institute of Radio Engineers*, vol. 40, no. 2, pp. 180–184, 1952.

[4] N. W. Ashcroft and N. D. Mermin, *Solid State Physics*, Brooks Cole, Pacific Grove, Calif, USA, 1st edition, 1976.

[5] H. Němec, P. Kužel, and V. Sundström, "Far-infrared response of free charge carriers localized in semiconductor nanoparticles," *Physical Review B*, vol. 79, no. 11, Article ID 115309, 2009.

[6] S. Lucyszyn, "Investigation of anomalous room temperature conduction losses in normal metals at terahertz frequencies," *IEE Proceedings—Microwaves, Antennas and Propagation*, vol. 151, no. 4, pp. 321–329, 2004.

[7] B. B. Yang, M. P. Kirley, and J. H. Booske, "Theoretical and empirical evaluation of surface roughness effects on conductivity in the terahertz regime," *IEEE Transactions on Terahertz Science and Technology*, vol. 4, no. 3, pp. 368–375, 2014.

[8] D. M. Pozar, *Microwave Engineering*, John Wiley & Sons, Hoboken, NJ, USA, 4th edition, 2012.

[9] S. P. Morgan Jr., "Effect of surface roughness on eddy current losses at microwave frequencies," *Journal of Applied Physics*, vol. 20, no. 4, pp. 352–362, 1949.

[10] E. Hammerstad and O. Jensen, "Accurate models for microstrip computer-aided design," in *Proceedings of the IEEE MTT-S International Microwave Symposium Digest*, pp. 407–409, Washington, DC, USA, May 1980.

[11] H. Braunisch, X. Gu, A. Camacho-Bragado, and L. Tsang, “Off-chip rough-metal-surface propagation loss modeling and correlation with measurements,” in *Proceedings of the 57th Electronic Components and Technology Conference (ECTC ’07)*, pp. 785–791, Reno, Nev, USA, June 2007.

[12] L. Tsang, X. Gu, and H. Braunisch, “Effects of random rough surface on absorption by conductors at microwave frequencies,” *IEEE Microwave and Wireless Components Letters*, vol. 16, no. 4, pp. 221–223, 2006.

[13] X. Gu, L. Tsang, H. Braunisch, and P. Xu, “Modeling absorption of rough interface between dielectric and conductive medium,” *Microwave and Optical Technology Letters*, vol. 49, no. 1, pp. 7–13, 2007.

[14] X. Gu, L. Tsang, and H. Braunisch, “Modeling effects of random rough interface on power absorption between dielectric and conductive medium in 3-D problem,” *IEEE Transactions on Microwave Theory and Techniques*, vol. 55, no. 3, pp. 511–517, 2007.

[15] X. Gu, L. Tsang, and H. Braunisch, “Estimation of roughness-induced power absorption from measured surface profile data,” *IEEE Microwave and Wireless Components Letters*, vol. 17, no. 7, pp. 486–488, 2007.

[16] X. Gu, *Modeling effects of random rough surface on conductor loss at microwave frequencies [Ph.D. thesis]*, University of Washington, Seattle, Wash, USA, 2006.

[17] N. M. Ridler and R. A. Ginley, “IEEE P1785: a new standard for waveguide above 110 GHz,” *Microwave Journal: Cables & Connectors Supplement*, 2011.

Journal of
Engineering

The Scientific World Journal
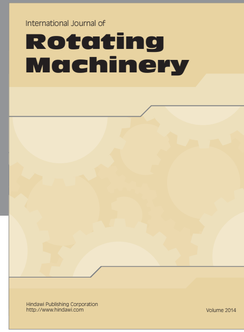
International Journal of
Rotating Machinery
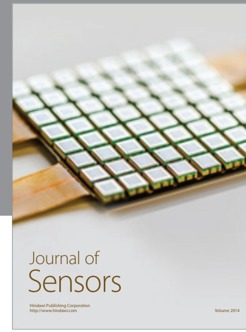
Journal of
Sensors
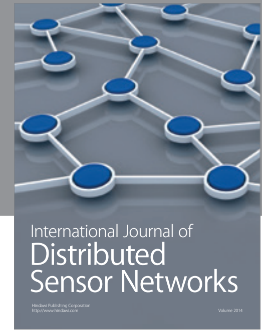
International Journal of
Distributed Sensor Networks
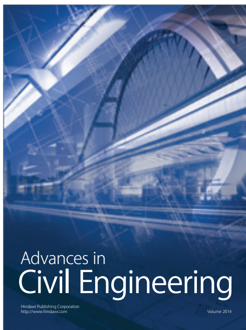
Advances in
Civil Engineering

Hindawi
Submit your manuscripts at
http://www.hindawi.com
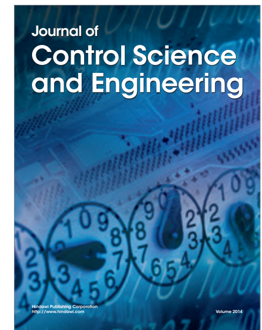
Journal of
Control Science and Engineering

Journal of
Robotics

Journal of
Electrical and Computer Engineering
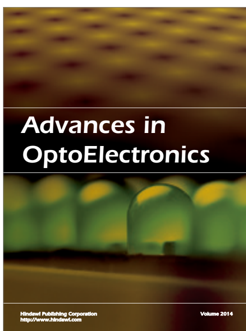
Advances in
OptoElectronics

VLSI Design

International Journal of
Navigation and Observation
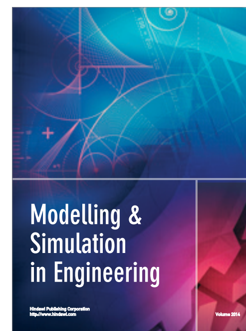
Modelling & Simulation in Engineering

International Journal of
Aerospace Engineering

International Journal of
Chemical Engineering
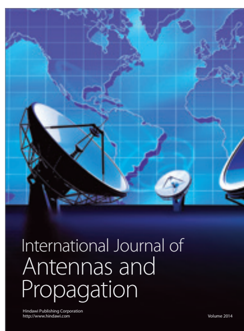
International Journal of
Antennas and Propagation
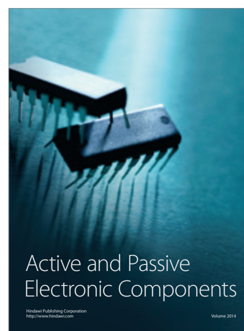
Active and Passive
Electronic Components
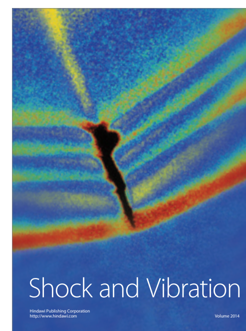
Shock and Vibration
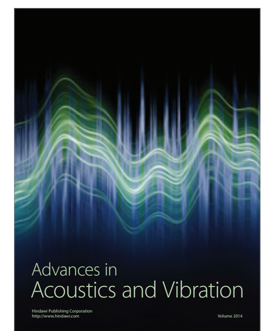
Advances in
Acoustics and Vibration